Near Field and Far Field Optical Properties of Plasmonic Nanocylinders

A thesis submitted towards partial fulfilment of
BS-MS Dual Degree Programme

by

MOHIT RAGHUWANSHI

under the guidance of

Dr. G.V. PAVAN KUMAR

Assistant Professor, IISER Pune

Indian Institute of Science Education and Research
Pune

Certificate

This is to certify that this thesis entitled 'NEAR FIELD AND FAR FIELD OPTICAL PROPERTIES OF PLASMONIC NANOCYLINDERS" submitted towards the partial fulfilment of the BS-MS dual degree programme at the Indian Institute of Science Education and Research Pune represents original research carried out by " MOHIT RAGHUWANSHI" at "IISER PUNE", under the supervision of "Dr. G.V. PAVAN KUMAR" during the academic year 2011-2012.

Student
Mohit
Raghuwanshi

Supervisor
G.V. Pavan
Kumar

Publications

1. Plasmonic nanocylinders arranged in Fibonacci number chain: Excitation angle-dependent optical properties Mohit Raghuwanshi, G.V. Pavan Kumar (under review 2012)

Acknowledgements

There are many people to whom I am very thankful. Above all I would especially like to thank Dr. G.V. Pavan Kumar for his valuable guidance, support and motivation in every meeting. I am highly thankful to IISER Pune for providing all the required library and computer resources. I am also very thankful to Arindam Dasgupta and Parthapratim Patra for their help in simulations. I am extremely grateful to my parents and sisters for supporting and encouraging me every now and then. I am also very thankful to all my friends of 2007 batch for distracting and taking me for tea every now and then.

Abstract

In this report we have studied the near field and the far field plasmonic properties of gold nanocylinders arranged linearly in a Fibonacci number chain and compared the results with those arranged in a conventional geometry. Assigning the radius of first two nanocylinders as 10nm, we have arranged five gold nanocylinders linearly with radii varying according to Fibonacci numbers and compared the optical properties with conventional geometry. Using FEM simulation we explored the near field distribution and the far field radiation pattern of the two geometries for various excitation angles. Our study reveals significant backscattered intensity in the far field radiation pattern for excitation angles along the chain for Fibonacci geometry, which was otherwise absent in conventional geometry. A systematic variation in near field enhancement is observed as a function of excitation angles which could guide us to tune Raman enhancement by changing the angle of excitation. We have obtained the maximum near field enhancement in the gap of two largest nanocylinders which is in contrast to the results obtained in the self similar chain of nanostructures. In addition we have explored the polarization dependent plasmonic properties of 1D silver nanowires and observed the strong dependence of incident polarization on propagation of surface plasmon polaritons.

Contents

Chapter 1

Introduction

1.1 Literature Survey

Research in interaction of light and a system of metallic nanocylinders has been at its peak in the past few years demonstrating enhancement of Raman scattering in the near fields as high as 10^{12} [1, 2]. Generation of these plasmonic properties strongly depend on the shape, size and the dielectric environment involved in the system [3] and change for a system of two or more metallic nanoparticles in close proximity, acting as a potential area of research [4]. This extraordinary enhancement is due to the coupling of Localized Surface Plasmons (LSPs) which gives rise to high electric field enhancement and generates what is known as electromagnetic hot spots in the gaps between nanoparticles in dimer [5] leading to applications in SERS and single molecule spectroscopy [6]. From single nanoparticle to assemblies and chains of nanoparticles various geometries of gold and silver nanoparticles are studied extensively for propagation and localization of light [7-11]. Among them chains of metallic nanoparticles have acquired a huge attention in recent years leading to many interesting applications including waveguides below diffraction limit, optimized SERS [7, 12-15], construction of integrated nanophotonic devices [16, 17], optical data storage systems [18-20], and biological sensing [11, 21]. Periodic linear structures like Self similar chain of metallic nanostructures have a wide range of applications including high local field enhancement, nano-optical detection, Raman characterization, nano focusing and manipulation of Light at nanometer scale and many more [9, 22-24]. Strong localization arising due to deterministic aperiodic structures is proven to have biological applications in enhancing sensitivity of a protein monolayer as small as tens of angstroms[25]. Linear chains of metallic nanostructures also have been extensively studied for their applications in

near field coupling and electromagnetic transport [7, 8, 26-30].

Most of the studies on linear chains till now have considered uniform size of metallic nanostructures [29, 31, 32]. Apart from conventional regular [8] or periodic array of metallic nanostructures, deterministic aperiodic plasmonic arrays (with some specific aperiodicity) have also captured attention in interesting applications like designing of sub wavelength optical fields on chip scale devices [33]. Hence it would be interesting to explore and compare optical properties of unconventional geometries to that of conventional one. Hence in this report we have explored the near field and far field optical properties of gold nanocylinders arranged in a linear geometry with size varying according to Fibonacci number [34]. Their comparison with the conventional chain of nanocylinders shows some unfamiliar results which were found absent in conventional chain geometry.

Self similar arrangement of metallic nanostructures used by [9, 23] presents the maximum enhancement of electromagnetic fields around the smallest nanostructure. In contrast to this result we have found the electromagnetic fields enhancement to be maximum in between the gaps of largest nanocylinders. In our current study we have arranged the radius of five consecutive gold nanocylinders in a Fibonacci number array and compared the plasmonic properties with conventional geomtry using FEM numerical method . Conventionally we have used the first two radius of the Fibonacci chain as 10nm and the surface to surface distance between consecutive nanocylinders to be 5nm. Radius for conventional geometry was chosen to be 25nm.

1.2 Plasmonics

Surface of metals such as Gold, Silver, Copper etc. are filled in a sea of conduction electrons and ions, together the term is called the Plasma. Oscillation of the free electron gas density on the surface of metal is called the Plasma oscillations and the quantum unit is called Plasmons [37]. Illumination of light on these surfaces may give rise to collective coherent oscillations of electron density at the metal-dielectric interface, quantized unit commonly known as surface plasmons [37]. When the wavelength of incident light matches the wavelength of the oscillation of surface plasmons, then the electrons resonate with the incident frequency resulting in the reduced scattered intensity due to coupling with surface plasmons giving rise to a phenomenon called Surface Plasmon Resonance (SPR) [37]. Interaction of photons and nanoparticles forms a wide range of study called nanophotonics; 'plasmonics' constitute the major part of nanophotonics exploring confinement of electromagnetic fields of the order of wavelength of incident light and smaller [40]. Metal-

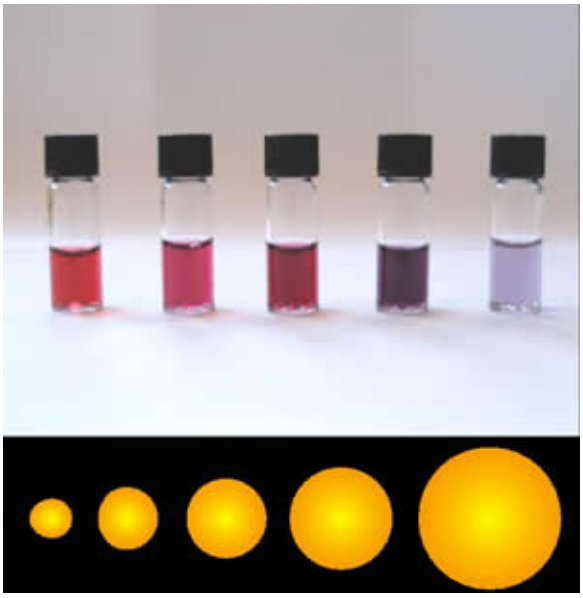

Figure 1.1: Different size solutions of Gold nanoshells .[83]

lic nanoparticles have large surface to volume ratio hence more number of electrons resides on the surface giving rise to SPR in large extent hence this phenomenon is strongly observed in gold and silver nanoparticles [80]. In fact different color solutions of gold and silver nanoparticles at visible light are one of the fascinating consequences of SPR [80]. Besides the formation of fascinating different color solution of metallic nanoparticles plasmonics have a wide range of applications in SERS and bio sensing in which metal nanoparticle could be used to enhance electric field enhancement around DNA molecule or protein [41]. Plasmonic circuits could help in designing of ultra fast interconnect chips that could work at speed as high as the speed of light beside the current limited transfer speed [42]. Metamaterials are negative refractive index materials which could be used for optical cloaking [43, 44] and solar cells is another future application of plasmonics [45]. One of the major challenges in plasmonics is the difficulty in confining light at nanoscale due to optical diffraction limit [42]. A nanoparticle dimer is formed when two nanoparticles are brought close together at a surface to surface distance of around few nanometers. Metallic nanoparticle dimers shows some extraordinary enhancement under the illumination of visible light and is thus useful for many application purposes. Local field enhancement and surface plasmon resonance of asymmetric metallic nanocylinders pairs have a huge application in focusing and manipulation of Light at nanometer scale [22].

We investigated the Near Field and Far Field for a gold nanoparticle chain

arranged in a Fibonacci number array using Finite Element Method (FEM) analysis by RF module of COMSOL 3.5a Multiphysics Modeling Software.

1.2.1 Near field and far field

Near fields and far fields for a system observed at nanoscale regime can basically be represented by Fresnel number.

Fresnel number is defined as

$$N = \frac{a^2}{L\lambda}$$

Where, a is the radius of the aperture, l is the wavelength of light, L is the distance of the screen from the aperture. Far Field region is defined as the region where N<<1. For N<<1 Fraunhoffer diffraction occurs, in this region the wave is only dependent on the angle from the source and independent of the distance from the source. Source of any shape can be considered as a point source while observing wave in this region. Near field region is defined as the region where N≥1. This is characterized by Fresnel diffraction. This is the region within few wavelengths from the aperture, where evanescent wave due to excitation of the surface plasmons is still strong [47].

1.2.2 Dielectric Constant

All metals exhibit dispersive properties i.e. their dielectric function (both the real and imaginary part) depends on the incident frequency. Dielectric constant plays a major role in the interaction of photon with metals. Optical phenomenon of electromagnetic wave like attenuation, reflection, refraction and polarization can be explained and derived using analytic expression of dielectric constant.

Assuming an incoming electromagnetic wave having electric field of the form $E = E_0 \exp(kz - i\omega t)$ an expression for dielectric constant in the case of absence of any external charge density can be derived as follows [53].

Maxwell's Equations for no external charge density can be written as:

$$\nabla.\mathrm{E} = 0 \qquad \ldots(1)$$

$$\nabla.\mathrm{H} = 0 \qquad \ldots(2)$$

$$\nabla \times \mathrm{E} = -\tfrac{1}{\mathrm{c}}\tfrac{\partial \mathrm{H}}{\partial \mathrm{t}} \qquad \ldots(3)$$

$$\nabla \times \mathrm{H} = \tfrac{4\pi}{\mathrm{c}}\mathrm{j} + \tfrac{1}{\mathrm{c}}\tfrac{\partial \mathrm{E}}{\partial \mathrm{t}} \qquad \ldots(4)$$

from the above two equations (3) & (4) we get

$$\nabla \times (\nabla \times \mathrm{E}) = \tfrac{\mathrm{i}\omega}{\mathrm{c}}(\tfrac{4\pi\sigma}{c}E - \tfrac{i\omega}{c}E) \qquad \ldots(5)$$

where,

$$\sigma = \frac{\sigma_0}{1-i\omega\tau};\ \sigma_o = \frac{ne^2\tau}{m} \quad \ldots(6)$$

From (5)

$$-\nabla^2 \mathrm{E} = \frac{\omega^2}{c^2}(1 + \frac{4\pi i\sigma}{\omega})\mathrm{E} \quad \ldots(7)$$

The above equation has the form of the usual wave function with the term in the paranthesis given by $\varepsilon(\omega)$ (dielectric constant) and τ is the relaxation time

$$\varepsilon(\omega) = 1 + \frac{4\pi i\sigma}{\omega}$$

Above equation can be simplified to :

$$\varepsilon(\omega) = 1 - \frac{\omega_p^2}{\omega^2 + i\gamma\omega} \quad \ldots(8)$$

Where ω_p is the plasma frequency and given by: and $\gamma = 1/\tau$; τ is the relaxation time

$$\omega_p = \sqrt{\frac{4\pi ne^2}{m}} \quad \ldots(9)$$

Equation (8) consist of a real part and an imaginary part which can be seperated applying rationalisation to above formula which finally gives as:

Real part

$$\varepsilon_1(\omega) = 1 - \frac{\omega_p^2\tau^2}{1 + \omega^2\tau^2} \quad \ldots(9)$$

And Imaginary Part as

$$\varepsilon_2(\omega) = \frac{\omega_p^2\tau}{\omega(1 + \omega^2\tau^2)} \quad \ldots(10)$$

1.2.3 Refractive index (n):

$$\mathrm{n} = \frac{c}{v_{(medium)}} = \frac{1}{\sqrt{\mu_0\varepsilon_0}} \cdot \sqrt{\mu_0\varepsilon_0} \cdot \sqrt{\mu_{med}\varepsilon_{med}}$$

$$\mathrm{n} = \sqrt{\mu_{med}\varepsilon_{med}} = \sqrt{\varepsilon_{med}} \quad \ldots(11)$$

(considering cases only for non-magnetic media hence taking μ(media) = 1) [81]

Hence the refractive index of a medium is proportional to the dielectric function of the medium thus is also complex. The two parts real and complex of the reafractive index can be represented as;

$$\mathrm{n} = n + i\kappa \qquad \ldots(12)$$

Here the real part of the refractive index (the ordinary refractive index n) determines the phase speed and the imaginary part (κ) determines the amount of absorption loss of the electromagnetic wave through the material [81]. Using equations (9), (10), (11) we can obtain an expression for refractive index in terms of frequency and also the real and imaginary parts of the refractive index in terms of the real and imaginary parts of the dielectric constant as:

$$n = \tfrac{1}{\sqrt{2}}\sqrt{(\varepsilon_1 + \sqrt{\varepsilon_1^2 + \varepsilon_2^2})} \qquad \ldots(13)$$

$$\kappa = \tfrac{1}{\sqrt{2}}\sqrt{(-\varepsilon_1 + \sqrt{\varepsilon_1^2 + \varepsilon_2^2})} \qquad \ldots(14)$$

The above two equations shows that the real and complex parts of the refractive index are not totally independent. Also the real and imaginary part of the dielectric constant can also be expressed in form of the two parts of the refractive index as:

$$\varepsilon_1 = n^2 - \kappa^2$$
$$\varepsilon_2 = 2n\kappa \qquad \ldots(15)$$

1.2.4 Attenuation constant:

Considering a harmonic wave travelling in z direction in a medium of refractive index 'n' having the form $E = E_0 \exp i(kz - \omega t)$, where k is the wave vector in the medium and is given by:

$$k = \tfrac{2\pi}{\lambda_{(med)}} = \tfrac{2\pi}{\lambda n} = \mathrm{n}\tfrac{2\pi}{\lambda} = \tfrac{\omega(n+i\kappa)}{c}$$

Substituting this value in the wave equation

$$E = E_0 \exp i((n + i\kappa)\frac{\omega}{c}z - \omega t)$$

$$E = E_0 \exp(-\frac{\kappa\omega}{c}z) \cdot \exp i(n\frac{\omega}{c}z - \omega t)$$

Thus the electric field decays exponentially with the distance in the medium. Intensity of the wave is given by $I = EE^*$. Therefore the expression of Intensity can be writen as:

$$I = E_0^2 \exp(-\frac{2\kappa\omega}{c} z)$$

According to Lambert-Beer's law we have the relation of intensity as propagation distance in the medium as $I = I_0 e^{-\alpha z}$, Where a is the attenuation constant. Comparing the above two equations we get

$$\alpha = \frac{2\kappa\omega}{c} \quad \ldots (16)$$

Since the attenuation constant is a function of the imaginary part of refractive index hence it is also a function of the two parts of the dielectric constant (κ in eq.14). Eq. (16) directly shows that the imaginary part of the refractive index (κ) is reponsible for the attenuation of the wave in the medium. Because κ is in turn directly related to ε_2(img. part of dielectric), it can further be extended that the imaginary part of the dielectric function is responsible for the attenuation of the wave in the medium. For the non transmission case i.e. the cases which we are interested in (for example - interaction of metals with visible light) we can say that the real part of the dielectric function $\varepsilon_1$represents the reflectivity of light at the interface.

1.2.5 Real and Imaginary parts of the dielectric function

For large frequencies close to ω_p , the product $\omega\tau >> 1$, which leads to negligible damping as given by (10), the real part of the dielectric function dominates ($\varepsilon_1 >> \varepsilon_2$)and therefore in this region, equation (8) simplifies to:

$$\varepsilon(\omega) = 1 - \frac{\omega_p^2}{\omega^2} \quad \ldots (17)$$

The above equation can be used for unreal cases for undamped free electron plasma. However practically speaking, for the case of noble metals

in this frequency regime is completely altered by interband transitions (discussed in the next section), leading to an increase in the imaginary part of the dielectric function and hence increase in absorption of the electromagnetic wave.

For small frequencies we have $\omega\tau << 1$, Hence the Imaginary part of the dielectric function dominates ($\varepsilon_2 >> \varepsilon_1$). From eqs. (13) & (14) it comes out that the real and imaginary part of refractive index are approximately same. This region is predominantly absorptive.

1.2.6 Surface Plasmon Polaritons (SPPs)

When Surface Plasmons couple with a photon, the resulting excitation is called a surface plasmon polariton (SPP) [35]. On a metal dielectric interface when light is impinged on the metal the resulting fields decays exponentially as a function of distance because of Ohmic effects and can be written as [35].

$$E_{SP}(x,z) = E_0 e^{ik_{sp}x - k_z|z|}$$

Where K_{SP} is the SPP wave vector which depends on the incident frequency and the system parameters and can be written as:

$$K_{SP}^2 = (\frac{\omega}{c})^2 \frac{\epsilon_i \epsilon_m}{\epsilon_i + \epsilon_m}$$

Above equation is also known as the dispersion relation and is plotted in the figure (1.2). Straight line shows the light line. The decay length for the surface plasmon can be calculated using the imaginary part of the SPP wave vector (as imaginary part is responsible for the attenuation of the field) and is equal to

$$L_{SP} = |2\, Im\, k_{SP}|^{-1} \qquad \ldots (18)$$

As can be seen from the figure, there is no electromagnetic wave propagation until the applied frequency equals the plasma frequency of the metal. And for further increase in frequency the above plotted curve is expected for a metal following Drude model. The dashed line here represents the light line i.e. applied frequency is directly proportional to its wave vector in vacuum. It can be observed from the above figure that plasma dispersion takes place for all the frequencies above plasma frequency.

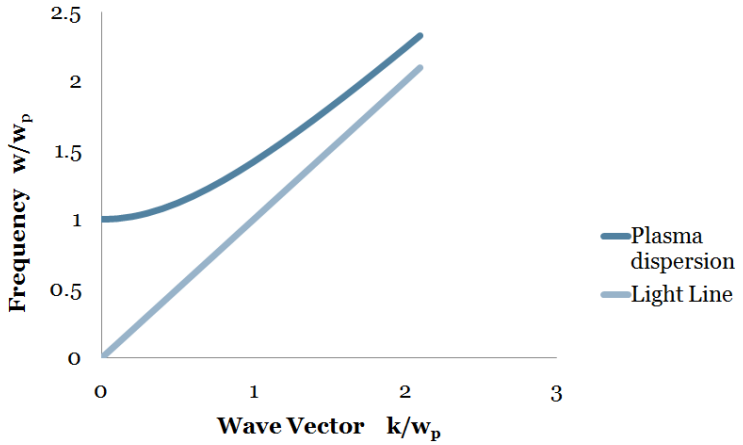

Figure 1.2: The dispersion relation of a free electron gas

1.2.7 Localized Surface Plasmon (LSPs)

In contrast to propagating modes, surface plasmons also exist in what is called bound modes such excitations taking place in bounded geometries are called localized surface plasmons [36]. Geometries such as metallic nanoparticles and metallic nanostructures are very commonly used for excitation of LSPs. Different color solutions of gold and silver nanoparticles fascinated everyone from centuries is a typical example of LSP phenomenon. Unlike surface plasmons in the bulk media, surface plasmons depend strongly on the size and shape of the particles when considered at the nanoscale. Nanoparticles have very large surface to volume ratio resulting in greater electron density confinement on the surface of nanoparticles as compared to bulk compact volume. Hence number of conduction electrons interacting with the incoming electromagnetic wave is increased by a large extent resulting in enhanced interaction.

1.2.8 Johnson and Christy values for dielectric function

Dielectric functions of gold and silver are plotted in fig 1.3:

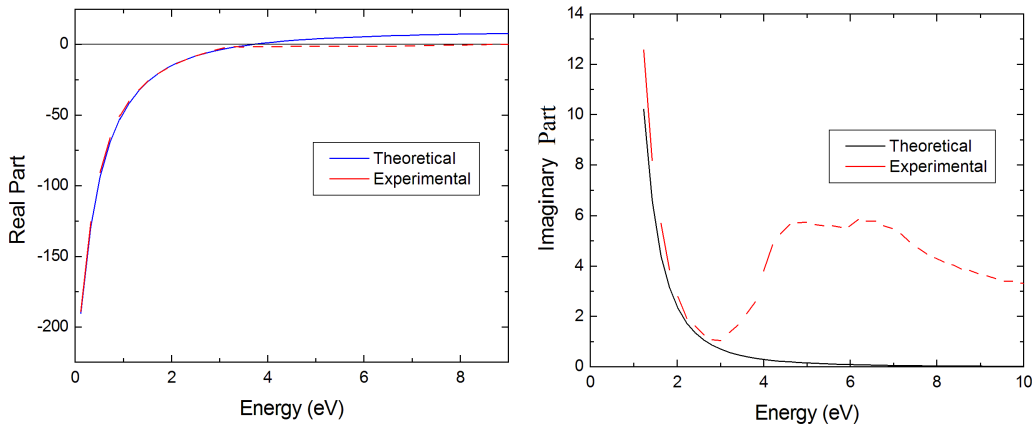

Figure 1.3: Dielectric function $\varepsilon(\omega)$) of the free electron gas (solid line) fitted to the literature values of the dielectric data for gold [Johnson and Christy, 1972] (dots).

From fig 1.3 we can deduce that drude model fits to the experimental data for low frequencies. In the case of gold the drude model is not valid above the boundary of near IR and Visible. This can be explained by interband transitions taking place at the metal's surface.

1.2.9 Interband Transitions

When light is illuminated on any metallic surface, the electrons in the metal can possibly make transition from one level to another, these type of transitions are called Interband transitions. These transitions can occur as soon as energy of the photons ($\hbar\omega$) in the incident light exceeds , $E_{n'}(k) - E_n(k)$ for some k and for two bands n and n', where $E_n(k)$ is below the fermi level (so that such an electron is available for excitation) and $E_{n'}(k)$ is above the fermi level (so that the final electronic level is not made unavailable by the Pauli principle) [82]. As already seen in the above section that drude model fails to explain the behavior of metal-light interaction at higher frequencies, however theory of Interband transitions explains the paradox. When the frequencies are small enough, the interband transitions are unlikely to occur, but as the frequencies are increased after the interband threshold, electrons start making transitions from lower energy level to higher energy level and hence electrons doesn't obey Drude's law, and hence the two curves does not overlap at higher frequencies. Also some other effects like intraband transtions (transitions within same band) may take place.

Chapter 2

Methods

Near field and far field optical properties of metallic nanocylinders are thoroughly studied and practiced by various research groups using both theoretical [10, 22, 45-48] and experimental methods [31, 49]. Electrodynamic simulation techniques are very helpful in providing a deeper understanding of the light matter interactions and also suggest implementation of appropriate changes that could be useful for the experiment and hence is very useful to guide the experiment in a better direction. In addition numerous cases and conditions could be solved using simulations very easily which are difficult when accessed using experiment.

In our current study we have used RF module of COMSOL 3.5a MULTIPHYSICS modeling software for two dimensions which uses FEM numerical technique for calculation of near field distribution and far field radiation. We have currently focused more on FEM and described a short introduction to other numerical techniques.

2.1 Numerical Techniques

2.1.1 Finite Difference Time Domain (FDTD)

The basic principle of FDTD is to replace the derivates in the Maxwell's curl equations by finite differences and then solving them in the time domain [50]. The idea of FDTD is computing E field and H field at each and every point in the geometry defined. FDTD traditionally use the Drude-Lorentz model (eq.19) for the frequency dependent permittivity response for materials and can thus cover a wide range of frequency response even for the ones which are not yet experimentally found [51, 52]

$$\varepsilon_\omega = \varepsilon_\infty - \frac{\omega_d^2}{\omega(\omega + i\gamma d)} - \frac{\triangle\epsilon.\Omega_l^2}{(\omega^2 - \Omega_l^2) + i\Gamma_l\omega} \quad \ldots.(19)$$

Where ω the incident frequency, ϵ the permittivity and other constants are fitted accordingly using the experimentally obtained values. Results can be visualized using softwares which take the Fourier transform of the time domain signal corresponding to scattered electric field and magnetic fields distributions.

2.1.2 Discrete Dipole Approximation (DDA)

Exact solutions to Maxwell's equations are only available for simplified symmetric geometries like sphere, infinite cylinders etc. DDSCAT uses discrete dipole approximation to simulate light scattering of electromagnetic wave due to arbitrary shaped particles. Each object defined in DDA is divided into arrays of small cubic elements. On illumination of electromagnetic wave, these elements redistribute charges on their surface creating a dipole moment and acting like dipoles. For an individual dipole we have the radiated field as given in [53, 54]. The sum of all the fields (fields due to scattering by other dipoles) can be written together in a matrix form A_{ij} [55]. The most fundamental function of DDSCAT is to calculate this matrix and solve for scattering cross sections using following equation [56]

$$\sigma_{sca} = \frac{k}{E_i^2} \int_{dS} |E_{scattered}(r').\hat{r}|^2 dS$$

One big advantage of using this technique is it allows calculation of multi sized particles in a single simulation and can simulate any arbitrary shape.

2.1.3 T-Matrix Method

T-Matrix method is widely used computational technique for calculation of light scattering by non-spherical particle and system of such particles. For problems involving light matter interaction, the components of the scattered radiation in some way are related to the components of the incident radiation and the operator in the matrix form relating the two is called the T-matrix.

$$\begin{bmatrix} a_n^{scattered} \\ b_n^{scattered} \end{bmatrix} = \begin{bmatrix} T_{11} & T_{12} \\ T_{21} & T_{22} \end{bmatrix} \begin{bmatrix} a_n^{incident} \\ b_n^{incident} \end{bmatrix}$$

Here the matrix consisting of T's terms is the T-matrix and $a_i^{scattered}$, $b_i^{scattered}$ are the components of scattered radiation and $a_i^{incident}$,$b_i^{incident}$ are

the components of incident radiation. Elements of T matrix are determined by matching the boundary conditions with the solutions obtained by solving Maxwell's equations and thus depend on refractive index of the particle and the surrounding medium, size of the particle and wavelength of the electromagnetic wave [55].

2.1.4 Finite Element Method (FEM)

FEM is a numerical technique which solves and gives approximate solutions for integral equations and partial differential equations. Numerical solutions even in very complicated cases can be easily solved using this technique which can be applied to a wide number of numerical problems involving electrodynamics, mechanics, thermodynamics, chemical physics and many more. In our case we have used the RF module of COMSOL Multiphysics Modeling software which uses FEM simulation technique in solving problems involving light matter interaction.

The first and very basic step of FEM is dividing a large (or small depending on reference) complicated structure or object into several elements which are quite easier to manage and then reconnects all of them at discrete points called nodes giving rise to a set of algebraic equations, this process is called generation of Mesh or preprocessing [57]. This process usually takes longer time for extra fine boundaries and hence can also be done using Computer Aided Design (CAD) which makes the process more convenient. Below is an example of coarse mesh, normal mesh and finer mesh constructed using COMSOL 3.5a FEM software, figure 2.1 shows small triangular meshes generated on surface of a circular object with sharp points as the nodes. In order to get more accurate and detailed results mesh can be made finer compromising with the simulation time [55].

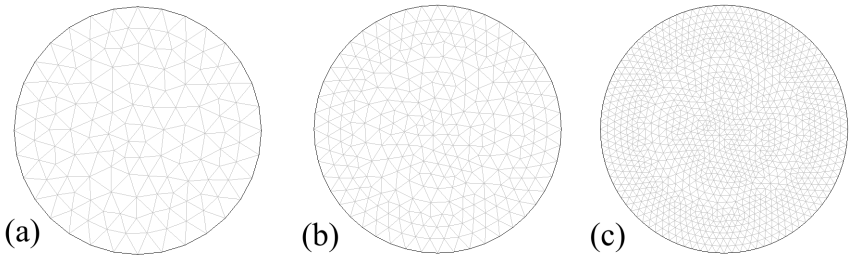

Figure 2.1: Different Mesh sizes (a) coarse (b) normal (c) fine

Second step is the analysis of the dataset prepared after preprocessing which involves solving of system of linear or non-linear equations in matrix

form (eq 20) using input created by the preprocessor.

$$K_{ij}u_j = f_i \qquad \ldots (20)$$

Where u is the displacement and f is the externally applied force at the ith nodal point. The formation of K matrix depends on the parameters chosen from the element library and the input constraints. The K matrix is solved for every small mesh element individually so large number of mesh elements results in increased simulation time. In fact one given problem can be solved using the same code for different materials just by changing the input material from the materials library; this is one of the best advantages of FEM.

Third step is the post processing of obtained solution in which the solution which is obtained in a matrix form is simulated in a graphical display which is extremely helpful in visualizing the results. In the earlier days, the user was required to list in large numbers generated by the code whereas modern codes and commercial softwares give results in many desired form including contour plots, arrow plots, 3D plots, boundary plots etc showing a very clear and detailed picture of the result. FEM simulations are one of the best for calculation of geometries involving curved surfaces and hence are considered one of the most reliable simulation techniques. On the other hand slow computation for 3D geometries is a big disadvantage in FEM, typically it takes three minutes to solve for a single frequency of normal mesh in 3 dimensions (for 1GHz processor, 1GB RAM, Dual Core) and thus one has to compromise between the computation time and the accuracy of the results.

Perfectly Matched Layers (PML): While attributing the outermost boundary one has to make sure that there are no unnecessary back scattering and reflections from the user defined boundary itself. This problem can be solved by introducing a PML region covering the outermost boundary. PML's are absorbing layers which is used to solve problems involving free boundaries, the most important point of having PML is the scattered outgoing waves from the object entering the PML region is completely absorbed while the incident wave is allowed to pass without any absorption [58].

Example of a 3D simulation in COMSOL 3.5a: Propagation of surface plasmons in silver nanowire.

Steps towards this simulation are shown below:

Preprocessing:

1) Defining geometry:

a) Draw a cylinder (silver nanowire) 2μm long with 56nm radius.

b) Draw a block (substrate) touching cylinder of appropriate dimensions.

c) Draw boundary (medium) of finite dimensions (in form of block) in order to contain the geometry.

d) Draw another boundary (PML) slightly bigger than above (in form of block) with center coinciding with above boundary.

e) Draw a hypothetical cylinder on one end of the wire (as shown in fig 2.2 below)

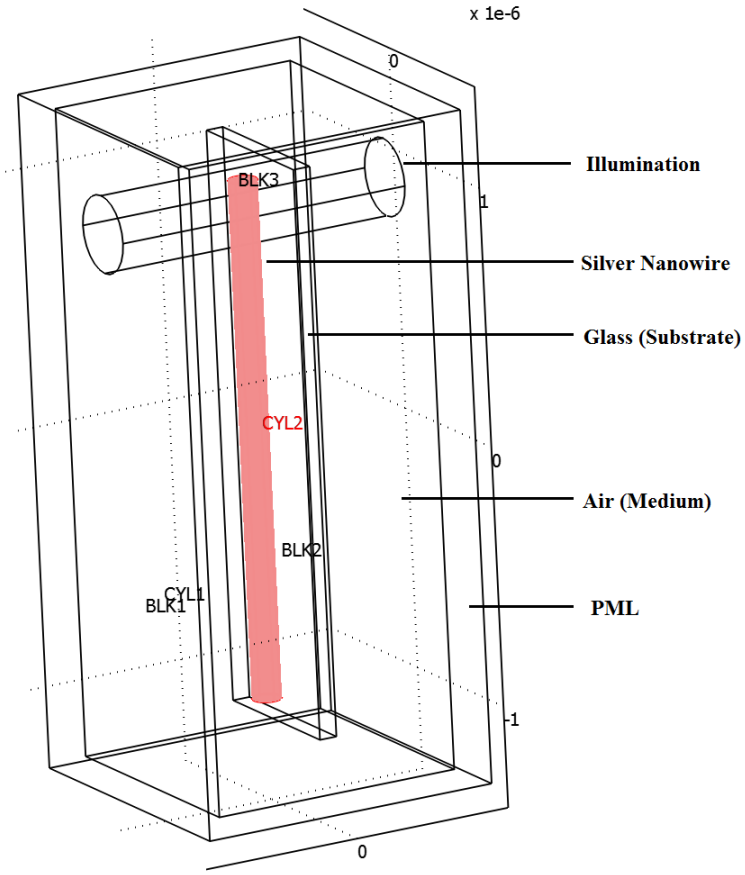

Figure 2.2: 3D geometry of silver nanowire in COMSOL

2) Subdomain Settings:

a) Addition of dielectric values of silver nanowire. Imported from Johnson and Christy experimentally determined values [52].

b) Check all the PML absorption for PML subdomain.

3) Boundary Settings:

a) Apply 'scattering boundary condition, plane wave illumination' to the circular boundaries of illumination cylinder (as shown in fig 2.2).

b) Apply Impedance boundary condition to the outermost PML boundary.

c) Apply continuity to all other boundaries.

4) Mesh and Other Parameters:

a) Change Mesh parameters accordingly in Mesh properties and Initialize Mesh

b) Specify wavelength = 633nm in scalar variables section.

c) Click on Solve.

After clicking on solve, the system solves the problem

Post processing:

After the solution is obtained there are several parameters which can be obtained both quantitatively and analytically e.g. distribution of Electric field (x,y,z, norm), Magnetic field (x,y,z, norm), Energy density (Electrical, Magnetic, Total), Far Field radiation patter, extinction spectra etc. These outputs can also be visualized in various types of plot (subdomain, boundary, contour, arrow etc).

2.2 Calculation of Extinction Spectra

The near field and Far field spectra of metal nanoparticle chains were calculated using the RF-Module of COMSOL 3.5a Multiphysics modeling software in two dimensions. Entire simulation was performed over a wavelength sweep of 400nm to 900nm i.e. mostly in the visible regime which also contains in the SPR wavelength for gold ($\approx$ 520nm). Far Field scattering efficiency on a spherical boundary is given by [59].

$$Q_{scat} = \frac{1}{\pi r_2^2 E_{inc}^2} \frac{1}{R_f^2} \int |E_{far}|^2 R_f^2 . d\Omega$$

Where R_f is the radius of the far field boundary chosen, E_far is the scattered electric field on boundary at R_f distance from center, E_inc is the incident electric field amplitude. One key advantage in using Comsol is that it automatically considers the term R_f^2 while perfoming boundary integrations giving finally the extinction efficiency multiplied by some constant factor. Hence scattering efficiency calculation can be easily done in Comsol by just defining E_far at boundary and calculating the integration over line (for 2D) or over surface (for 3D). Similarly Absorption efficiency could be determined by integrating the time averaged resistive heating (U_{av}) [59]. But because we

are considering the case when absorption is far less significant than scattering we can approximate extinction efficiency to be equal to scattering efficiency.

2.3 Geometry used:

Geometry used in our current study is represented in fig 2.3. Fig.2.3 (a) shows the Fibonacci number array used, numbers (above nanocylinders) represent the ratio of radius of nanocylinders to be used in order to form a Fibonacci array. Traditional Fibonacci number array extends to infinity but we utilize the first five terms for our calculations. Gold nanocylinders are arranged symmetrically with respect to x-axis on the x-axis (here x-axis corresponds to the axis containing the chain of nanocylinders). Fig 2.3 (b) represents conventional regular chain geometry of gold nanocylinders.

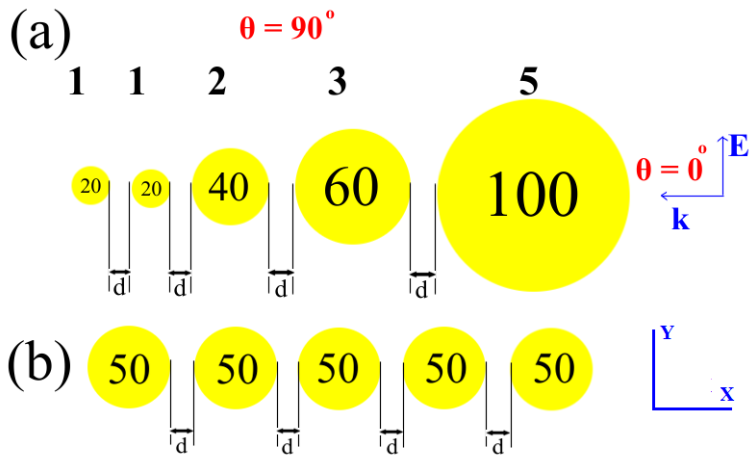

Figure 2.3: Geometry representing arrangement of gold nanocylinders according to Fibonacci numbers. The numbers inside the nanocylinders represent their diameter in nm. Arrows E and k represent electric field polarization and propagation vectors respectively and θ represents the excitation angle. (b) Conventional chain of gold nanocylinders (CC) of 50nm diameter, 'd' is the constant gap between the nanocylinders and is equal to 5nm

We restrict our simulation to two dimensions which assumes the gold nanocylinders extend infinite in length towards the positive and negative z-axis, radius of the nanocylinders are chosen to be minimum 10nm and maximum 50nm which vary according to the Fibonacci number array as shown in the figure. Surface to surface distance between two consecutive nanocylinders are kept constant to be 5nm throughout the simulation. The whole geometry

was kept in air as the medium (refractive index = 1) symmetrically spread in a region of 1.2m in diameter with respect to center of the geometry. Far fields are calculated on the outermost boundary of the medium i.e. at 600nm from center of the geometry. Perfectly Matched Layer (PML) region is used at the boundary of the medium in order to absorb unwanted back scattering of light due to boundaries.

In current study we have used TM polarized plane wave having propagation vector and electric field parallel to the plane of the geometry. Conventionally the illumination direction is chosen from the side containing nanocylinder with the largest radius, as shown in Fig.2.3 by blue arrow, θ in the figure represents the angle convention used in the geometry. Dielectric function of gold nanocylinders as a function of incident wavelength is adapted from Johnson and Christy [52].

Chapter 3

Results and Discussions

In our current report we have studied the near field and far field optical properties of FC geometry and compared them with CC geometry. Some very interesting and additional observations are made in case of FC geometry which were quite absent in CC geometry. In addition we have also explored propagation of surface plasmon polaritons on surface of silver nanocylinders excited at particular wavelength.

3.1 Propagation and Localization of Light on Metal Nanoparticle Chains

Previously it is well studied and shown by Dal Negro and co-workers [25, 33, 60-62] that deterministic aperiodic nanostructures could explore unusual optical properties which are otherwise absent in conventional geometries. Here in this report we have investigated the near field and far field plasmonic properties generated due to the interaction of TM Polarized plane wave and linear chain of gold nanocylinders whose radii are arranged according to Fibonacci number sequence with same surface to surface distance. As shown in this report we have obtained the far field spectrum for the geometry as a function of incident angles and incident wavelengths demonstrating potential applications in nano focusing and bio sensing [20-22]. An extraordinary near field enhancement in the gap between the largest nanocylinders caused due to the coupling of localized Plasmon resonance has wide number of applications in SERS [12, 13]. Self similar arrangement of metallic nanostructures used by [9, 23] presents the maximum enhancement of electromagnetic fields around the smallest nanostructure. Exact geometry used is clearly shown in the methods section (fig 2.3).

3.1.1 Extinction Spectra for various excitation angles

Interaction of an electromagnetic wave with a particle or chain of particles results in absorption and scattering collectively the term called extinction, efficiency depending mainly on the geometry, dielectric function, wavelength of incident light and other parameters used in the system. Figure (3.1 (a and c) shows the plot of extinction spectra for different angles (integral of the square of the norm electric field observed at the medium boundary, that is 600nm from the center) versus wavelength for FC geometry and CC geometry respectively. Figure (3.1 (b & d) shows the excitation wavelength (wavelength corresponding to maximum extinction at boundary of the medium) Vs Angle of incidence for FC and CC geometry respectively. Angle convention used is as shown in the figure i.e. 0^o is attributed to the side containing the largest nanocylinder. Excitation wavelength for a single gold nanocylinder lies around 522nm, although excitation wavelength for 0^o and 180^o is observed at 522nm whereas a nice variation is observed for other oblique incident illumination angles. Also an asymmetry for the FC geometry peak wavelength (fig 3.1 b) is visible and a continuous gradual increase in the peak wavelength is observed for an increase in the angle of excitation, whereas for CC geometry we observed comparatively a rapid increment. This property of FC geometry is derived from the asymmetric arrangement and can be potentially used in generation of electromagnetic hot spot from any desired wavelength.

As can be inferred from the figure 3.1, the peak wavelength is observed to be red shifted as the angle of illumination sweeps from 0^o to 90^o and then the pattern reverses as it reaches 0^o . The above pattern can be explained using classical harmonic oscillator problem as we are not taking into account for the quantum effects which arise on further decreasing the length scale. Restoring forces due to interaction of light and matter doesn't really depend on the angle of illumination when considered individually but when considered collectively, consideration of angle of illumination is very critical because of coupling between neighboring cylinders [63]. When the TM polarized plane wave is illuminated along the x-axis, electric field is on the Y axis thus oscillating the cylinders along Y-axis leading to stronger coupling between them and thus the resonance shifts to higher frequency or lower wavelength. Whereas while considering the perpendicular illumination electric field is on the x-axis thus oscillation of cylinders is on the x-axis leading to a reduced coupling due to neighbor shifting the resonance to lower frequency or higher wavelength. This mechanism is known as the near field coupling mechanism [64].

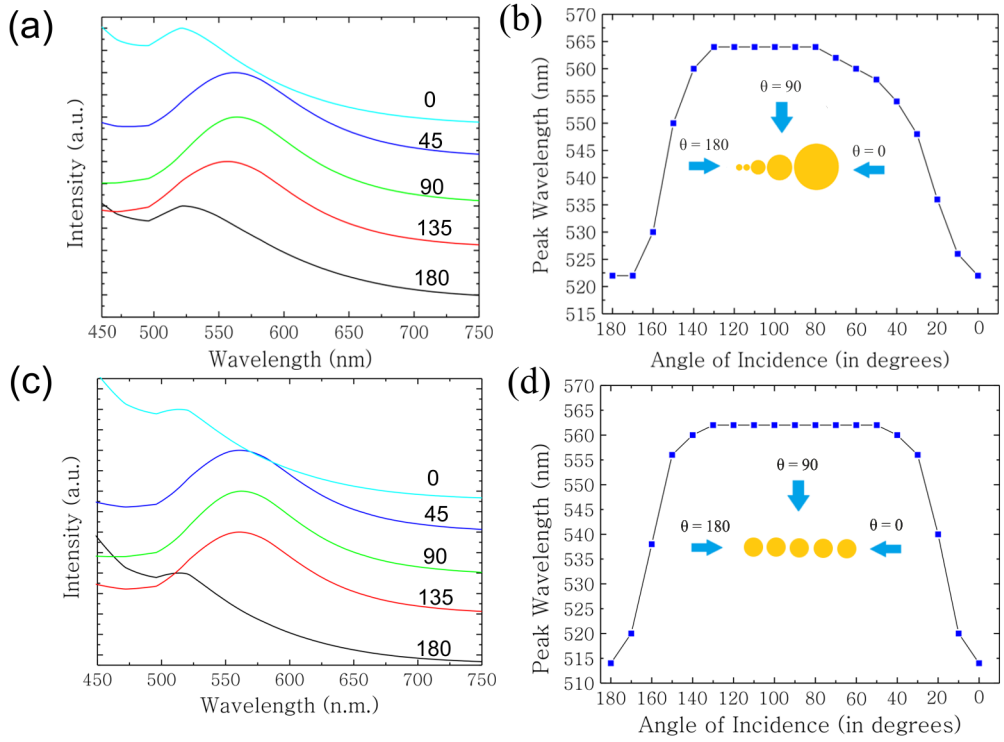

Figure 3.1: (a) Far-field intensity spectra for different excitation angles in FC geometry; (b) Variation of excitation wavelength as function of excitation angles in FC geometry. (c) Far-field intensity spectra for different excitation angles in CC geometry; (d) Variation of excitation wavelength as function of excitation angles in CC geometry

3.1.2 Far Field Radiation Pattern

Here we have shown the far field radiation pattern for the two geometries and discussed the back scattering efficiency and forward scattering efficiency between the two. Angle of incidence plays a key role in evaluation of far field spectra for a system of two or more nanoparticles.

Figure 3.3 basically represents the polar plot of angular pattern of intensity (arbitrary units) as a function of arc length on the outer boundary of the medium. Forward scattering and backward scattering due to the gold nanocylinders are quantitatively expressed in figure 3.3. Fig 3.3 (a-e) represents far field radiation pattern for FC geometry at different angles (as shown in fig) at wavelength corresponding to maximum far field. Angular sweep used was from 0^o to 180^o in steps of 45^o , because the geometry is symmetric with respect to x-axis we obtain similar symmetric results while

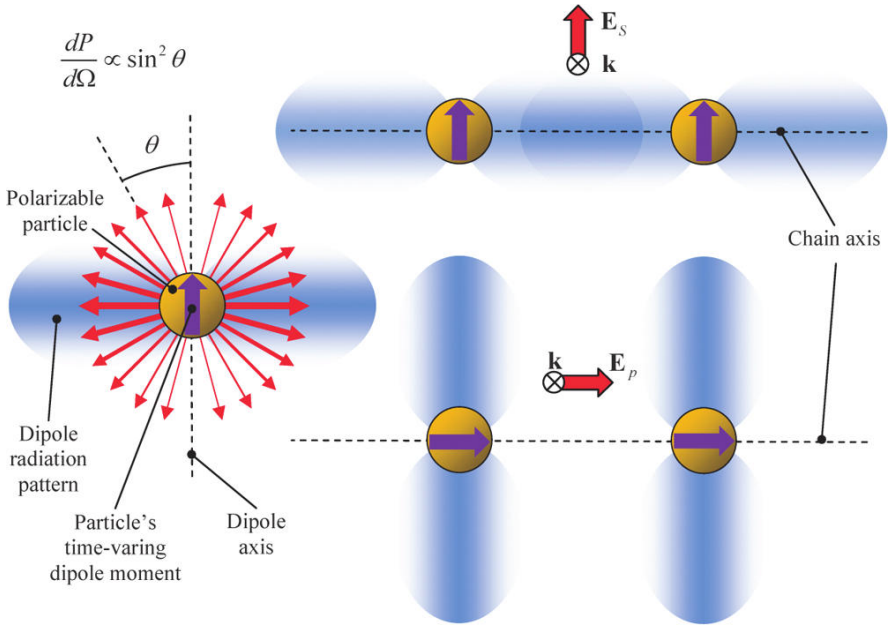

Figure 3.2: (Left) Radiation pattern of a dipole (arrow shows dipole moment direction). (Right) coupling in different polarization directions [63].

sweeping angles from 180^o to 360^o and hence not shown here. Forward and backward scattering calculations are particularly useful in focusing of light at nanoscale and also pave the way for better utilization of light. Calculation of forward and backward scattering at each wavelength gives an approximate idea about the transmission and reflection of light at that wavelength which might be quite useful in construction of highly efficient solar cells.

Figure 3.3 shows the far field radiation pattern for the two geometries FC (a-e) and CC (f-j) at five different excitation angles 0^o , 45^o , 90^o , 135^o , 180^o . As can be inferred from the figure, the forward scattering is always greater than the backward scattering except for the case of perpendicular illumination i.e. fig 3.3 (c, h). However it is also noticeable that for 45^o , 90^o and 135^o excitation angles the two geometries show similar response of forward scattering and backscattering. Whereas for 0^o and 180^o excitation angle significant backscattering in case of FC is noticeable as compared to CC in which it is completely absent. From this result we can deduce that in FC geometry radiation is not only coupled towards the forward direction but also in the backward direction. This is an interesting property of FC geometry which gives us an indication that a gradient in size of the nanoparticles could be exploited for backscattering.

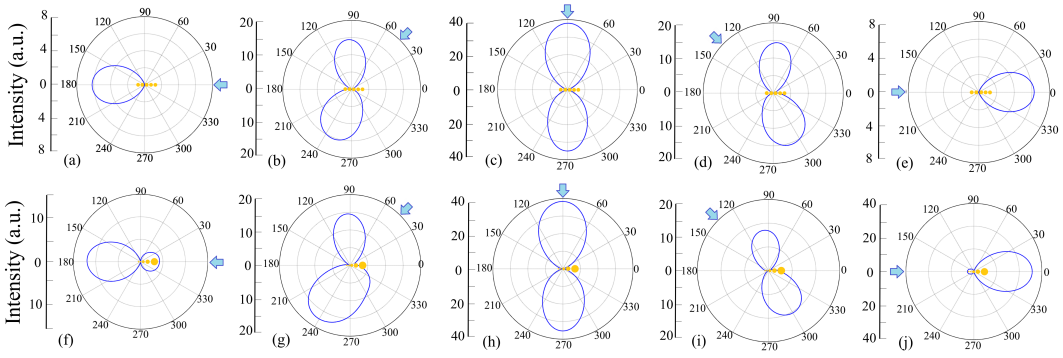

Figure 3.3: Far-field radiation pattern in FC geometry for excitation angles (a-e) 0, 45, 90,135, 180 degrees. Far-field radiation pattern in CC geometry for excitation angles (f-j) 0, 45, 90,135, 180 degrees.

3.1.3 Near Field Electric Distribution

So far we have discussed only the far field spectra and far field radiation pattern for the two geometries FC and CC. In fact near field optical properties of the two geometries depicts further interesting observations. In this section we will mainly discuss upon the near field enhancement and near electric field distribution for the two geometries.

Interaction of electromagnetic wave and a system of two or more nanostructures when placed in closed vicinity can give rise to electromagnetic hot spots. Analytical theory for electromagnetic interaction of touching nanoparticle dimers already exists [65] and also it is now well understood that the electric field near the vicinity of composite plasmonic nanostructures could be enhanced by a factor as high as 10^4 [66]. These enhanced electric fields explore its potential use in SERS (Surface Enhanced Raman Scattering). Controlling and tuning such large enhancements could be one of the critical issues. One of the best ways to tune and control these enhancements could be done by changing the angle of excitation [67-69]. Near field enhancement typically depends on the polarization and incident angle of the field, thus varying these two parameters and keeping the geometry same we can tune the near field.

In this report we have explored the near field distribution of electric field for different excitation angles (0, 45, 90, 135, and 180) for FC and CC geometry and compared the near field enhancements between them. Fig 3.4 (a-e) represents near field distribution for FC geometry and fig 3.4 (f-j) represents near field distribution for CC geometry. As can be seen in the figure, the maximum magnitude of near electric field for FC geometry varied from 5000

V/m at 90^o to 1000 V/m at 0^o whereas for CC geometry maximum magnitude of near electric field varied from 4800 V/m at 90^o to 600 V/m at 0^o . A common observation in both the geometry is that the near field enhancement monotonically increases till excitation angle reaches 90^o i.e. perpendicular illumination because as angle sweeps till perpendicular illumination coupling gets stronger due to increased dipole-dipole interaction and is maximum when nanocylinders are polarized in the direction perpendicular to their chain axis i.e. for 90^o illumination (see fig 3.2).

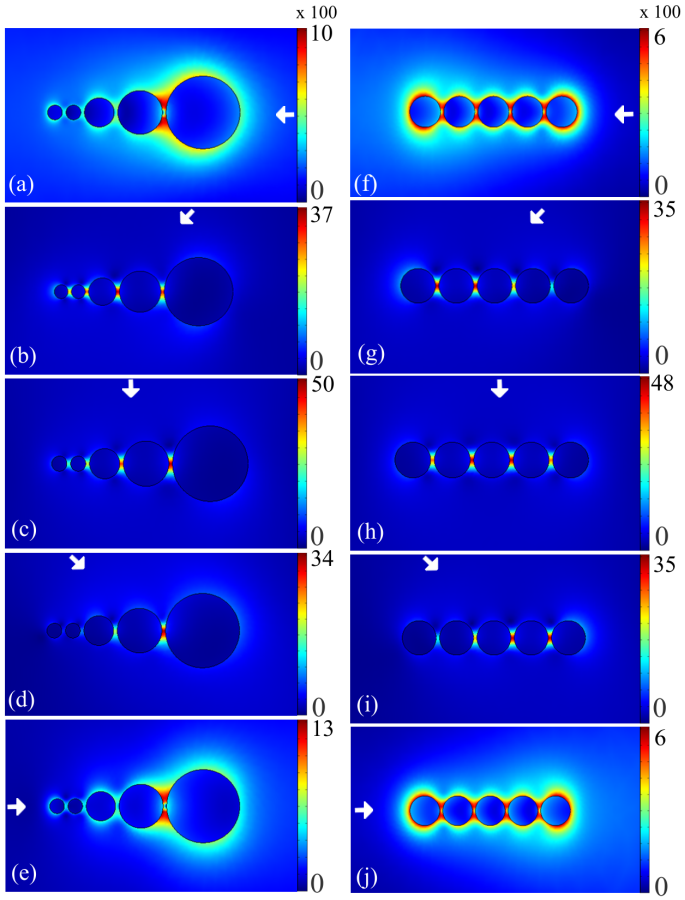

Figure 3.4: Near-field distribution for different excitation angles in FC and CC geometry. (a, b, c, d, e) represents near-field distribution in FC for 0, 45, 90, 135, 180 degree excitation angles, respectively; and (f, g, h, i, j) represent near field distribution of CC for 0, 45, 90, 135, 180 degree excitation angles, respectively. Color code represents magnitude of Electric field norm and arrow indicates the k vector.

3.1.4 Near Field Spatial Distribution

As observed in fig 3.4 the maximum and minimum values of electric field in the near field regime is almost same for both the geometries however a look at their spatial distribution shows generation of multiple electromagnetic hot spots as shown in fig 3.5 for 90^o excitation angle.

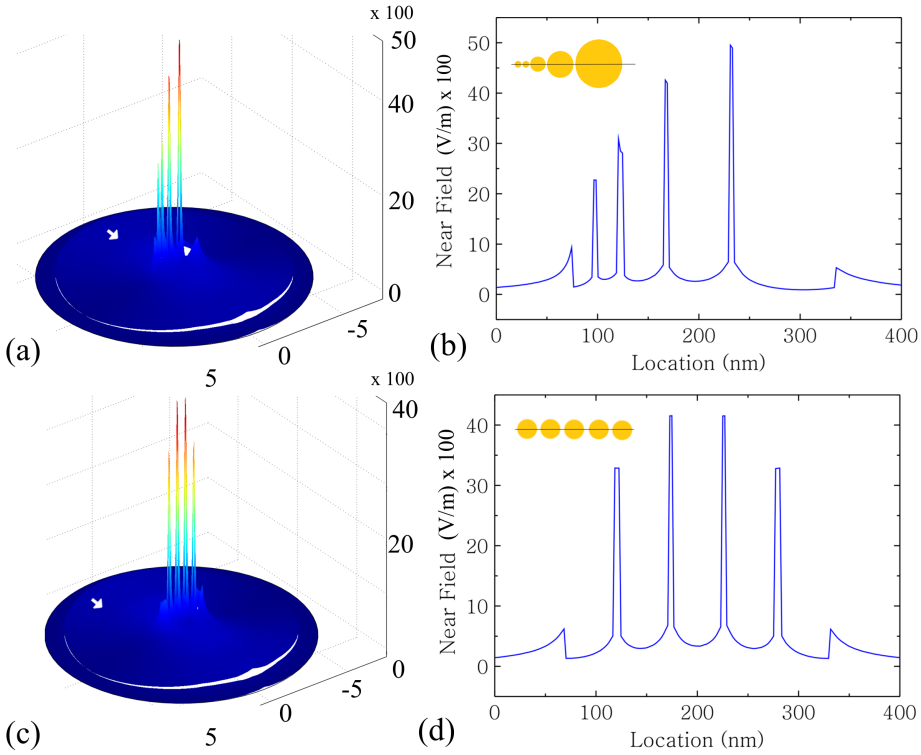

Figure 3.5: (a) 3D plot of near-field distribution in FC geometry for 90^o excitation; (b) magnitude of near-field as function of linear co-ordinate in FC geometry. (c) 3D plot of near field distribution in CC geometry for 90^o excitation; (d) magnitude of near-field as function of linear co-ordinate in FC geometry. Insets shows the geometry and relevant linear-coordinates.

Fig 3.5a represents the 3D projection of electric field distribution and fig 3.5b represents the near field enhancement as a function of linear coordinates along chain axis for FC geometry at 90^o excitation. We observed a nice gradient of near field enhancement for FC geometry and the enhancement is proportional to cylinder's size this is because of the coupling between localized surface plasmons (LSPs) for larger cylinders coupling is more. Whereas for CC geometry fig 3.5 (b&d) we observed an almost uniform enhancement

of multiple hot spots this is again because of the same size of individual nanocylinders near field enhancement is almost similar. However in spite of same size a slight variation is clearly visible in fig 3.5 (d), i.e. near field enhancement is maximum around the middle nanocylinders, this can again be explained using fig 3.2 that collective dipole radiation decays as $1/r^2$, hence maximum coupling of collective dipole radiation occurs at center. This is the scenario for 90^o illumination however we can tune the near field enhancement as a function of linear coordinates by changing the angle of excitation (as shown in fig 3.6).

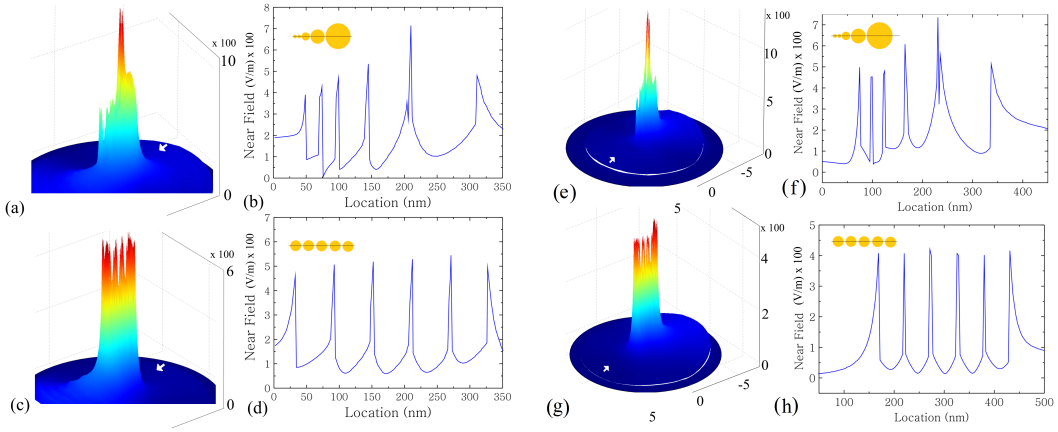

Figure 3.6: Near field distribution comparison for the illumination along chain axis. Illumination direction is shown by white arrow

As evidenced in fig 3.6 we can deduce that the near field enhancement can be tuned just by changing the angle of excitation. When nanocylinders are excited at angles different than perpendicular and parallel polarization, charges on the surface of nanocylinder redistributes them according to the incident angle and results in variation of near field enhancement.

3.1.5 Raman Enhancement

As we have observed in (fig.3.4) near field coupling in between localized surface plasmons (LSPs) can give rise to extraordinary electric field enhancements and results in creation of electromagnetic hot spots. Local field enhancements in such Plasmonic nanostructures are ideal sources to perform SERS. Raman enhancement factor can be calculated using the maximum near field observed in fig.3.4 (discussed in theory) for both the geometries at different angles as shown in fig 3.7.

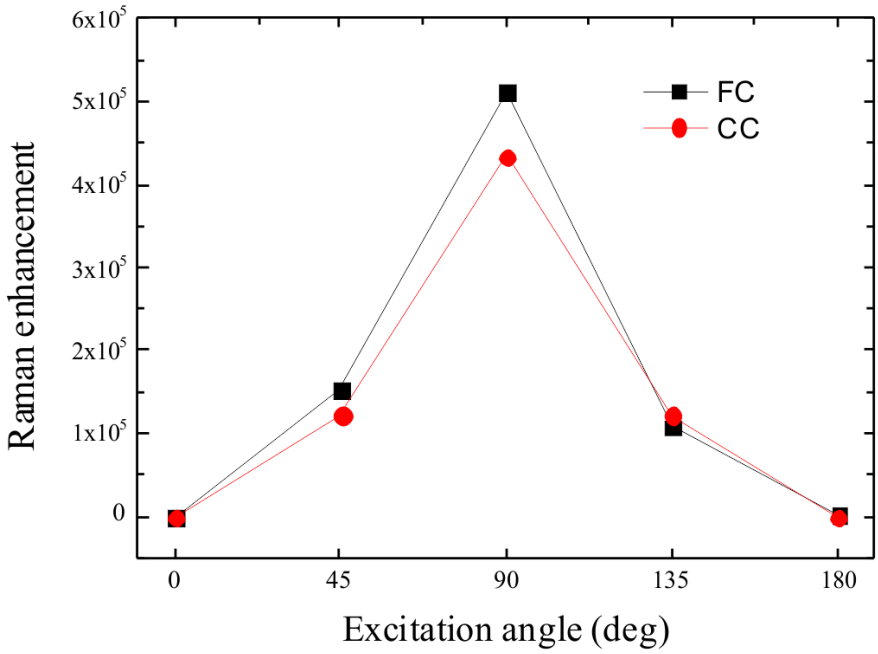

Figure 3.7: Raman enhancement in FC and CC geometries as a function of excitation angle

As can be inferred from fig 3.7, the maximum Raman enhancement for FC geometry is 5.1×10^5 and for CC it is 4.3×10^5 both observed at 90^o illumination. Minimum enhancement is observed for 0^o and 180^o which is consistent with fig 3.4 and again can be explained using dipole coupling model (fig 3.2). Another interesting consequence of the asymmetric arrangement of FC geometry is the asymmetry in Raman enhancement as can be seen in fig 3.7, a slight asymmetry is observed for FC as compared to CC which is completely symmetric.

3.1.6 Comparison with self similar chain

Self similar chain of nanospheres are thoroughly studied by some research groups [24] claiming the maximum near field enhancement around smallest nanostructure. Quite similar to FC geometry in Self similar chain also nanoparticles are arranged with a monotonic gradient in size. These are periodic chains in which surface to surface distance between two successive nanoparticles and size of next nanocylinder is directly proportional to the size of the nanoparticle [24]. In contrast to the results observed using self similar geometry we have obtained maximum enhancement around the largest nanocylinders (as shown in the figure below).

Hence a possible conclusion can be made that the location and magnitude of near field enhancement strongly depend on size of the geometry as well as on the periodicity of the geometry chosen.

3.2 Propagation of SPPs on continuous one dimensional Plasmonic nanostructures

Plasmonic nanowire can serve as waveguide for SPP propagation and can serve as a key component in designing photonic integrated circuits overcoming bandwidth limitations and limited data transmission rate in electronic circuits [11, 70-73]. SPPs when excited on plasmonic nanostructures (e.g. silver nanowire, nanoparticle chains etc) can travel distances as long as tens of nanometers [74-77]. Propagation of SPPs depends strongly on the dielectric property of metal and environment, wavelength of light as usual and also the polarization of the incident electromagnetic field is a key factor [78].

Here in this report we have demonstrated the propagation of SPPs on a $2\mu m$ long silver nanowire of radius 56nm using 3D RF module of COMSOL Multiphysics 3.5a, refer to fig(2.2). Throughout the simulation we have kept the incident wavelength to be equal to 633nm, as in case of experimental justification 633nm red laser is easily available, and the corresponding

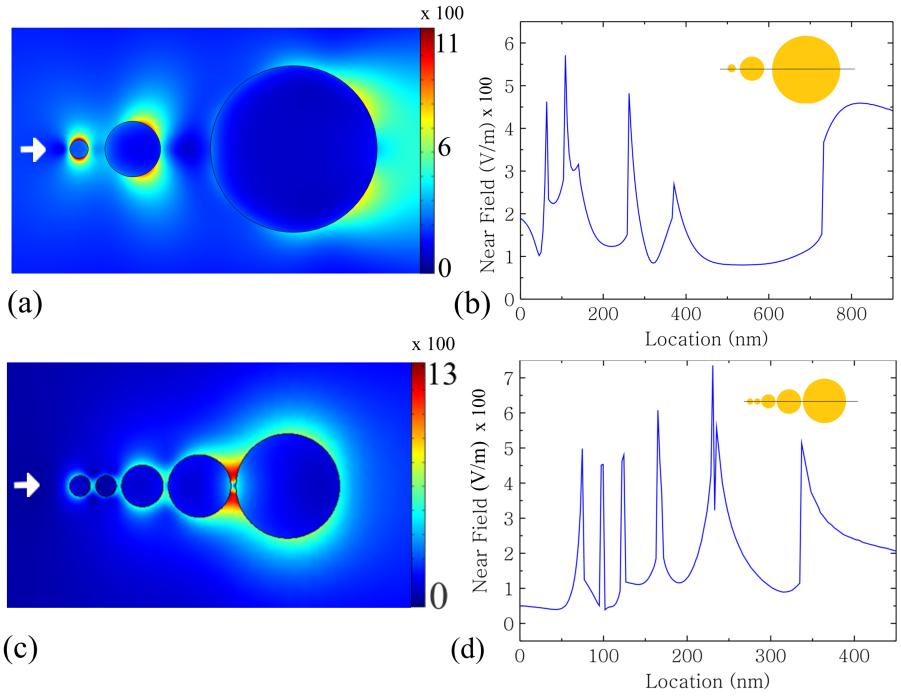

Figure 3.8: (a) Near field distribution for self similar geometry (b) Near field magnitude as function of linear coordinate along chain axis (c) Near field distribution for FC geometry (d) Near field magnitude as a function of linear coordinate along chain axis. Arrow shows the illumination direction.

refractive index is used for Ag metal [52]. One another reason for using single wavelength is the limited processor RAM and processing speed because wavelength sweep for small meshes might crash the system. Electric field is illuminated towards one of the end of the Ag nanowire and slice plot at nanowire's surface is used to visualize the propagation of SPPs.

As can be inferred from the above figure, for polarization along the wire axis (fig 3.9a) propagation of SPPs is clearly witnessed with minimum loss. End points of nanowire are accompanied with red dots (i.e. high electric fields) which give a clear implication of high transmission. In second case we saw minimal propagation of SPP for polarization perpendicular to nanowire axis (fig 3.9b) and also the end caps are not accompanied with significant electric field. We obtained contrasting results in the two cases; this is because polarization of electric field along the wire axis creates oscillation along the wire length which gets carried over towards other end, whereas for other case oscillation is perpendicular to the wire length resulting in minimal propagation along wire. The third case is very interesting in which we observe

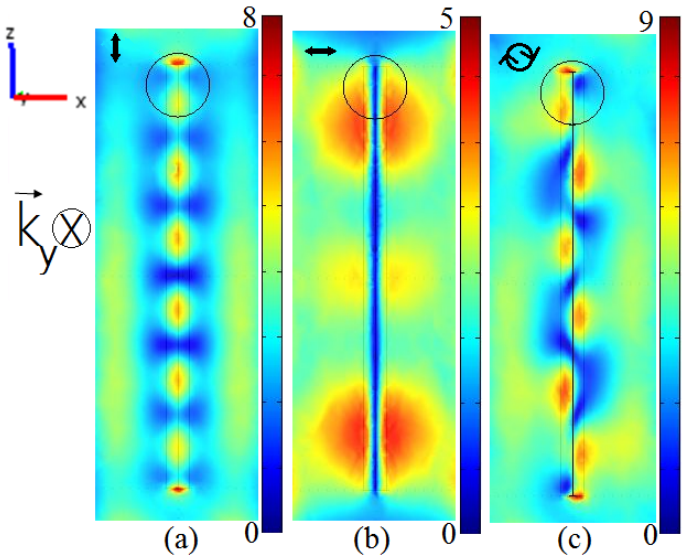

Figure 3.9: Slice plot for Ag nanowire representing near field distribution. Electromagnetic wave is incident towards Y-direction on the circle drawn with three different polarizations (a) Along Z-axis (b) along X-axis (c) circularly polarized. Double headed arrows represent the incident polarization.

propagation of chiral plasmons [79] on the surface of nanowire for circular polarization illumination. In this case the oscillation is along both parallel to the wire as well as perpendicular to the wire with equal amplitude. The formation of chiral plasmons at nanoscale regime could explore potential applications in probing of enantiomeric molecules at nanoscale [79].

Chapter 4

Conclusion

We have numerically explored the near field and far field excitation angle dependent optical properties of gold nanocylinders arranged in Fibonacci number chain (FC) geometry and compared the obtained results with the conventional chain geometry (CC). Comparison of Far field radiation pattern shows that a gradient in size of nanoparticles could give an enhanced amount of backscattered intensity for excitation angles along the chain of nanoparticles. We found that near field enhancement around the chains of metallic nanoparticles (both FC and CC) can be tuned by varying the angle of incidence which can be harnessed for applications in SERS and chip based nanophotonics devices. For perpendicular excitation in FC geometry we observed a gradient of near field enhancement around gold nanocylinders as a function of size with maximum enhancement around largest nanocylinder, this could be used in tuning of Raman enhancement as a function of size i.e. tuning both size and angle gives more flexibility for specific required enhancement. Comparison of near field enhancement for FC geometry and self similar geometry clearly indicates the difference in near field optical properties for periodic and a periodic nanostructures. Finally we studied the polarization dependence of propagation of SPPs along the silver nanowire chain and found that linear polarization along the wire axis could induce propagation of SPPs for few ums and is not significant for polarization perpendicular to the chain axis. In addition observation of chiral plasmon propagation was very fascinating to be observed for incident circular polarization.

4.1 Future Direction

Our angular dependent near field studies for different geometries explored alternative methods of fine tuning the near field enhancement. Hence any

amount of required value for field could be maintained and hence could be used as a source of electric field for photonic integrated circuits or photonic crystal waveguides, in which the applied field can be varied by fine tuning the angle of excitation. Our far field studies indicate that for FC geometry we get very continuous distribution of excitation wavelength for different excitation angles, hence could be a useful technique of absorbing maximum photons of any wavelength.

4.2 Drawbacks

We approximated our simulation for 2D geometry as because of limited computer resources it was very difficult to carry out wavelength dependent 3D simulations for curved geometries in COMSOL. Also we direclty substituted the values of dielctric constant for gold and silver as taken from Johnson and Christy values [1976], however dielectric properties at nanoscale might change.

References

1. Moskovits, M., Surface-enhanced spectroscopy. Reviews of Modern Physics, 1985. 57(3): p. 783-826.

2. Stockman, M.I., et al., Enhanced Raman scattering by fractal clusters: Scale-invariant theory. Physical Review B, 1992. 46(5): p. 2821-2830.

3. Trachuk, L.A., A.G. Melnikov, and N.G. Khlebtsov. Dependence of the optical properties of metal nanoparticles on the external dielectric medium: Effects of the particle size, shape, and structure. 2005.

4. Pileni, M.P., Nanocrystal self-assemblies: Fabrication and collective properties. Journal of Physical Chemistry B, 2001. 105(17): p. 3358-3371.

5. Ng, M.Y. and W.C. Liu, Local-field confinement in three-pair arrays of metallic nanocylinders. Optics Express, 2006. 14(10): p. 4504-4513.

6. Lal, S., et al., Tailoring plasmonic substrates for surface enhanced spectroscopies. Chemical Society Reviews, 2008. 37(5): p. 898-911.

7. Quinten, M., et al., Electromagnetic energy transport via linear chains of silver nanoparticles. Optics Letters, 1998. 23(17): p. 1331-1333.

8. Salerno, M., et al., The optical near-field of gold nanoparticle chains. Optics Communications, 2005. 248(4-6): p. 543-549.

9. Essone Mezeme, M., S. Lasquellec, and C. Brosseau, Subwavelength control of electromagnetic field confinement in self-similar chains of magnetoplasmonic core-shell nanostructures. Physical Review E - Statistical, Nonlinear, and Soft Matter Physics, 2011. 84(2).

10. Pavan Kumar, G.V., Near-field optical properties of silver nanocylinders arranged in a Pascal triangle. Appl. Opt., 2010. 49(36): p. 6872-6877.

11. Lal, S., S. Link, and N.J. Halas, Nano-optics from sensing to waveguiding. Nature Photonics, 2007. 1(11): p. 641-648.

12. Maier, S.A., et al., Local detection of electromagnetic energy transport below the diffraction limit in metal nanoparticle plasmon waveguides. Nature Materials, 2003. 2(4): p. 229-232.

13. Felidj, N., et al., Optimized surface-enhanced Raman scattering on gold nanoparticle arrays. Applied Physics Letters, 2003. 82(18): p. 3095-3097.

14. Maier, S.A., P.G. Kik, and H.A. Atwater, Observation of coupled plasmon-polariton modes in Au nanoparticle chain waveguides of different lengths: Estimation of waveguide loss. Applied Physics Letters, 2002. 81(9): p. 1714-1716.

15. Haynes, C.L., et al., Nanoparticle optics: The importance of radiative dipole coupling in two-dimensional nanoparticle arrays. Journal of Physical Chemistry B, 2003. 107(30): p. 7337-7342.

16. Ohtsu, M., et al., Nanophotonics: Design, fabrication, and operation of nanometric devices using optical near fields. IEEE Journal on Selected Topics in Quantum Electronics, 2002. 8(4): p. 839-862.

17. Kawazoe, T., et al., Demonstration of a nanophotonic switching operation by optical near-field energy transfer. Applied Physics Letters, 2003. 82(18): p. 2957-2959.

18. Liu, W.C., et al., Near-field images of the AgOx-type super-resolution near-field structure. Applied Physics Letters, 2001. 78(6): p. 685-687.

19. Tominaga, J., et al., Super-Resolution Near-Field Structure and Signal Enhancement by Surface Plasmons. Japanese Journal of Applied Physics, Part 2: Letters, 2001. 40(3 B): p. 1831-1834.

20. Liu, W.C., M.Y. Ng, and D.P. Tsai, Surface plasmon effects on the far-field signals of AgOx-type super resolution near-field structure. Japanese Journal of Applied Physics, Part 1: Regular Papers and Short Notes and Review Papers, 2004. 43(7 B): p. 4713-4717.

21. Anker, J.N., et al., Biosensing with plasmonic nanosensors. Nature Materials, 2008. 7(6): p. 442-453.

22. Ng, M.Y. and W.C. Liu, Local field enhancement of asymmetric metallic nanocylinder pairs. Journal of the Korean Physical Society, 2005. 47(SUPPL. 1): p. S135-S139.

23. Stockman, M.I., S.V. Faleev, and D.J. Bergman, Localization versus delocalization of surface plasmons in nanosystems: Can one state have both characteristics? Physical Review Letters, 2001. 87(16): p. 167401/1-167401/4.

24. Li, K., M.I. Stockman, and D.J. Bergman, Self-similar chain of metal nanospheres as an efficient nanolens. Physical Review Letters, 2003. 91(22): p. 227402/1-227402/4.

25. Lee, S.Y., et al., Spatial and spectral detection of protein monolayers with deterministic aperiodic arrays of metal nanoparticles. Proceedings of the National Academy of Sciences of the United States of America, 2010. 107(27): p. 12086-12090.

26. Girard, C. and R. Quidant, Near-field optical transmittance of metal particle chain waveguides. Optics Express, 2004. 12(25): p. 6141-6146.

27. Wei, Q.H., et al., Plasmon resonance of finite one-dimensional Au nanoparticle chains. Nano Letters, 2004. 4(6): p. 1067-1071.

28. Ghenuche, P., R. Quidant, and G. Badenes, Cumulative plasmon field enhancement in finite metal particle chains. Optics Letters, 2005. 30(14): p. 1882-1884.

29. Pinchuk, A.O. and G.C. Schatz, Nanoparticle optical properties: Far- and near-field electrodynamic coupling in a chain of silver spherical nanoparticles. Materials Science and Engineering B: Solid-State Materials for Advanced Technology, 2008. 149(3): p. 251-258.

30. Zou, S. and G.C. Schatz, Theoretical studies of plasmon resonances in one-dimensional nanoparticle chains: Narrow lineshapes with tunable widths. Nanotechnology, 2006. 17(11): p. 2813-2820.

31. Kravets, V.V., et al., Electrodynamic coupling in regular arrays of gold nanocylinders. Journal of Physics D: Applied Physics, 2012. 45(4).

32. Simsek, E., On the surface plasmon resonance modes of metal nanoparticle chains and arrays. Plasmonics, 2009. 4(3): p. 223-230.

33. Dal Negro, L., N.N. Feng, and A. Gopinath, Electromagnetic coupling and plasmon localization in deterministic aperiodic arrays. Journal of Optics A: Pure and Applied Optics, 2008. 10(6).

34. Zwillinger, D., CRC standard mathematical tables and formulae2011: CRC press.

35. Zayats, A.V. and I.I. Smolyaninov, Near-field photonics: Surface plasmon polaritons and localized surface plasmons. Journal of Optics A: Pure and Applied Optics, 2003. 5(4): p. S16-S50.

36. Vollmer, M. and U. Kreibig, Optical properties of metal clusters. Springer Ser. Mater. Sci, 1995. 25.

37. Maier, S.A., Plasmonics: fundamentals and applications2007: Springer Verlag.

38. Bantz, K.C., et al., Recent progress in SERS biosensing. Physical Chemistry Chemical Physics, 2011. 13(24): p. 11551-11567.

39. Atwater, H., The Promise of Plasmonics. Scientific American, 2007.

40. Cai, W., et al., Optical cloaking with metamaterials. Nature Photonics, 2007. 1(4): p. 224-227.

41. Pendry, J.B., D. Schurig, and D.R. Smith, Controlling electromagnetic fields. Science, 2006. 312(5781): p. 1780-1782.

42. Sakai, O. and K. Tachibana, Plasmas as metamaterials: A review. Plasma Sources Science and Technology, 2012. 21(1).

43. Loo, C., et al., Nanoshell-Enabled Photonics-Based Imaging and Therapy of Cancer. Technology in Cancer Research and Treatment, 2004. 3(1): p. 33-40.

44. D'Elia, G., et al., New method of far-field reconstruction from Fresnel field. Electronics Letters, 1984. 20(8): p. 342-343.

45. Ng, M.-Y. and W.-C. Liu, Local-field confinement in three-pair arrays of metallic nanocylinders. Opt. Express, 2006. 14(10): p. 4504-4513.

46. Li, Z., Z. Yang, and H. Xu, Comment on "Self-Similar Chain of Metal Nanospheres as an Efficient Nanolens". Physical Review Letters, 2006. 97(7): p. 079701.

47. Ng, M.Y. and W.C. Liu, Controlling surface plasmon excitation of pair arrays of metallic nanocylinders. Applied Physics A: Materials Science and Processing, 2007. 89(2): p. 391-395.

48. Lu, J.Y., et al., Multiple metallic-shell nanocylinders for surface-enhanced spectroscopes. Nanoscale Research Letters, 2011. 6(1): p. X1-7.

49. Zhang, K., et al., Composite soft-matter nanoscale objects: Nanocylinder-templated assembly of nanospheres. Soft Matter, 2009. 5(19): p. 3585-3589.

50. Kane, Y., Numerical solution of initial boundary value problems involving maxwell's equations in isotropic media. Antennas and Propagation, IEEE Transactions on, 1966. 14(3): p. 302-307.

51. Vial, A., et al., Improved analytical fit of gold dispersion: Application to the modeling of extinction spectra with a finite-difference time-domain method. Physical Review B - Condensed Matter and Materials Physics, 2005. 71(8).

52. Johnson, P.B. and R.W. Christy, Optical constants of the noble metals. Physical Review B, 1972. 6(12): p. 4370-4379.

53. Jackson, J.D., Classical Electrodynamics. Wiley1999, New York.

54. Bottcher, C.J.F., Theory of Electric Polarisation. Elsevier, 1973.

55. Parsons, J., et al., A comparison of techniques used to simulate the scattering of electromagnetic radiation by metallic nanostructures. Journal of Modern Optics, 2010. 57(5): p. 356-365.

56. Bohren, C.F. and D.R. Huffman, in Absorption and Scattering of Light by Small Particles2007, Wiley-VCH Verlag GmbH.

57. Roylance, D. Finite Element Analysis. 2001.

58. Berenger, J.P., A perfectly matched layer for the absorption of electromagnetic waves. Journal of Computational Physics, 1994. 114(2): p. 185-200.

59. Knight, M.W. and N.J. Halas, Nanoshells to nanoeggs to nanocups: Optical properties of reduced symmetry core-shell nanoparticles beyond the quasistatic limit. New Journal of Physics, 2008. 10.

60. Dal Negro, L. and S.V. Boriskina, Deterministic aperiodic nanostructures for photonics and plasmonics applications. Laser and Photonics Reviews, 2012. 6(2): p. 178-218.

61. Trevino, J., H. Cao, and L. Dal Negro, Circularly symmetric light scattering from nanoplasmonic spirals. Nano Letters, 2011. 11(5): p. 2008-2016.

62. Gopinath, A., et al., Photonic-plasmonic scattering resonances in deterministic aperiodic structures. Nano Letters, 2008. 8(8): p. 2423-2431.

63. Gozhenko, V.V., et al., Tunable resonance absorption of light in a Chain of gold nanoparticles. Journal of Physical Chemistry C, 2011. 115(18): p. 8911-8917.

64. Halas, N.J., et al., Plasmons in strongly coupled metallic nanostructures. Chemical Reviews, 2011. 111(6): p. 3913-3961.

65. Fernandez-Dominguez, A.I., S.A. Maier, and J.B. Pendry, Collection and Concentration of Light by Touching Spheres: A Transformation Optics Approach. Physical Review Letters, 2010. 105(26): p. 266807.

66. Kravets, V.G., et al., Cascaded Optical Field Enhancement in Composite Plasmonic Nanostructures. Physical Review Letters, 2010. 105(24): p. 246806.

67. Nikitin, A.Y., et al., Scattering of surface plasmon polaritons by impedance barriers: Dependence on angle of incidence. Physical Review B - Condensed Matter and Materials Physics, 2008. 77(19).

68. Shao, L., et al., Angle-and energy-resolved plasmon coupling in gold nanorod dimers. ACS Nano, 2010. 4(6): p. 3053-3062.

69. Park, C.H., J.W. Choi, and Y.H. Cho, Real-time surface plasmon resonance dispersion imaging with a wide range of incident angles and detection wavelengths. Applied Optics, 2010. 49(13): p. 2470-2474.

70. Akimov, A.V., et al., Generation of single optical plasmons in metallic nanowires coupled to quantum dots. Nature, 2007. 450(7168): p. 402-406.

71. Leosson, K., et al., Long-range surface plasmon polariton nanowire waveguides for device applications. Optics Express, 2006. 14(1): p. 314-319.

72. Oulton, R.F., et al., A hybrid plasmonic waveguide for subwavelength confinement and long-range propagation. Nature Photonics, 2008. 2(8): p. 496-500.

73. Zia, R., et al., Plasmonics: the next chip-scale technology. Materials Today, 2006. 9(7-8): p. 20-27.

74. Dickson, R.M. and L.A. Lyon, Unidirectional plasmon propagation in metallic nanowires. Journal of Physical Chemistry B, 2000. 104(26): p. 6095-6098.

75. Ditlbacher, H., et al., Silver nanowires as surface plasmon resonators. Physical Review Letters, 2005. 95(25).

76. Sanders, A.W., et al., Observation of plasmon propagation, redirection, and fan-out in silver nanowires. Nano Letters, 2006. 6(8): p. 1822-1826.

77. Fang, Y., et al., Remote-excitation surface-enhanced raman scattering using propagating ag nanowire plasmons. Nano Letters, 2009. 9(5): p. 2049-2053.

78. Li, Z., et al., Correlation between incident and emission polarization in nanowire surface plasmon waveguides. Nano Letters, 2010. 10(5): p. 1831-1835.

79. Zhang, S., et al., Chiral surface plasmon polaritons on metallic nanowires. Physical Review Letters, 2011. 107(9).

80. Sharma, V., K. Park, and M. Srinivasarao, Colloidal dispersion of gold nanorods: Historical background, optical properties, seed-mediated synthesis, shape separation and self-assembly. Materials Science and Engineering R: Reports, 2009. 65(1-3): p. 1-38.

81. Fox, M., Optical Properties of Solids2001, New York: Oxford University Press.

82. Kittel, C. and P. McEuen, Introduction to solid state physics. Vol. 7. 1976: Wiley New York.

83. Aleksandar Kondinski, kondinski.webs.com.